A Cryptic Site of Vulnerability on the Receptor Binding Domain of the SARS-CoV 2 Spike Glycoprotein — Source link ↗

M. Gordon Joyce, Rajeshwer S. Sankhala, Wei-Hung Chen, Misook Choe ...+18 more authors

Institutions: Walter Reed Army Institute of Research, Uniformed Services University of the Health Sciences, Leidos, National Institutes of Health

Related papers:

- Cryo-EM structure of the 2019-nCoV spike in the prefusion conformation.

- Structure, Function, and Antigenicity of the SARS-CoV-2 Spike Glycoprotein.

- A highly conserved cryptic epitope in the receptor binding domains of SARS-CoV-2 and SARS-CoV.

- SARS-CoV-2 Cell Entry Depends on ACE2 and TMPRSS2 and Is Blocked by a Clinically Proven Protease Inhibitor

- Human Monoclonal Antibody Combination against SARS Coronavirus: Synergy and Coverage of Escape Mutants

Share this paper:

View more about this paper here: https://typeset.io/papers/a-cryptic-site-of-vulnerability-on-the-receptor-binding-2hqcpr04j1

A Cryptic Site of Vulnerability on the Receptor Binding Domain of the SARS-CoV-2 Spike Glycoprotein

M. Gordon Joyce[1,2,3,7,*], Rajeshwer S. Sankhala[1,2,3,7], Wei-Hung Chen[1,2,3,7], Misook Choe[1,2,3,7], Hongjun Bai[1,2,3,7], Agnes Hajduczki[1,2,3,7], Lianying Yan[4], Spencer L. Sterling[4], Caroline E. Peterson[1,2,3,7], Ethan C. Green[1,4,7], Clayton Smith[5,6], Natalia de Val[5,6], Mihret Amare[1,3,7], Paul Scott[1,7], Eric D. Laing[4], Christopher C. Broder[4], Morgane Rolland[1,2,3,7], Nelson L. Michael[7], Kayvon Modjarrad[1,7,*]

[1]Emerging Infectious Diseases Branch, Walter Reed Army Institute of Research, Silver Spring, MD, USA.

[2]U.S. Military HIV Research Program, Walter Reed Army Institute of Research, Silver Spring, MD, USA.

[3]Henry M. Jackson Foundation for the Advancement of Military Medicine, Bethesda, MD, USA.

[4]Department of Microbiology and Immunology, Uniformed Services University, Bethesda, MD, USA, Bethesda, MD, USA.

[5]Center for Molecular Microscopy, Center for Cancer Research, National Cancer Institute, National Institutes of Health, Frederick, MD, USA.

[6]Cancer Research Technology Program, Frederick National Laboratory for Cancer Research, Leidos Biomedical Research Inc., Frederick, MD, USA.

[7]Center for Infectious Diseases Research, Walter Reed Army Institute of Research, Silver Spring, MD, USA.

*Correspondence: gjoyce@eidresearch.org (M.G.J) and kayvon.modjarrad.civ@mail.mil (K.M.)

SUMMARY

SARS-CoV-2 is a zoonotic virus that has caused a pandemic of severe respiratory disease—COVID-19—within several months of its initial identification. Comparable to the first SARS-CoV, this novel coronavirus's surface Spike (S) glycoprotein mediates cell entry via the human ACE-2 receptor, and, thus, is the principal target for the development of vaccines and immunotherapeutics. Molecular information on the SARS-CoV-2 S glycoprotein remains limited. Here we report the crystal structure of the SARS-CoV-2 S receptor-binding-domain (RBD) at a the highest resolution to date, of 1.95 Å. We identified a set of SARS-reactive monoclonal antibodies with cross-reactivity to SARS-CoV-2 RBD and other betacoronavirus S glycoproteins. One of these antibodies, CR3022, was previously shown to synergize with antibodies that target the ACE-2 binding site on the SARS-CoV RBD and reduce viral escape capacity. We determined the structure of CR3022, in complex with the SARS-CoV-2 RBD, and defined a broadly reactive epitope that is highly conserved across betacoronaviruses. This epitope is inaccessible in the "closed" prefusion S structure, but is accessible in "open" conformations. This first-ever resolution of a human antibody in complex with SARS-CoV-2 and the broad reactivity of this set of antibodies to a conserved betacoronavirus epitope will allow antigenic assessment of vaccine candidates, and provide a framework for accelerated vaccine, immunotherapeutic and diagnostic strategies against SARS-CoV-2 and related betacoronaviruses.

KEYWORDS

Coronavirus, COVID-19, SARS-CoV-2, Antibodies, Pandemic, Structural Biology, Receptor-Binding-Domain

HIGHLIGHTS

High resolution structure of the SARS-CoV-2 Receptor-Binding-Domain (RBD).

Recognition of the SARS-CoV-2 RBD by SARS-CoV antibodies.

Structure of the SARS-COV-2 RBD in complex with antibody CR3022.

Identification of a cryptic site of vulnerability on the SARS-CoV-2 Spike.

INTRODUCTION

The emergence of SARS-CoV-2 marks the seventh coronavirus to be isolated from humans, and the third to cause a severe disease—named COVID-19—after severe acute respiratory syndrome (SARS) and Middle East respiratory syndrome (MERS)(Munster et al., 2020). The rapid spread of SARS-CoV-2, and the grave risk it poses to global health, prompted the World Health Organization to declare, on 30 January 2020, the COVID-19 outbreak to be a public health emergency of international concern and on 11 March 2020 to be a pandemic(Wu et al., 2020; Zhou et al., 2020). As of 13 March 2020, there have been nearly 140000 SARS-CoV-2 infections and more than 5000 associated deaths reported across at least 100 countries. The rapidly evolving epidemiology of the pandemic and absence of licensed prophylactics or therapeutics for the disease have accelerated the need to elucidate the molecular biology of this novel coronavirus.

Although SARS-CoV-2 is a newly identified virus, it shares genetic and morphologic features with others in the *Coronaviridae* family, particularly those from the Betacoronavirus genus. The genome of the recently isolated SARS-CoV-2 shares 82% nucleotide identity with human SARS-CoV and 89% with bat SARS-like-CoVZXC21 (Lu et al., 2020). The spike (S) glycoprotein, in particular, bears significant structural homology with SARS-CoV compared to other coronaviruses such as MERS-CoV. Like SARS-CoV, the surface Spike (S) glycoprotein of SARS-CoV-2 binds the same host receptor, ACE-2, to mediate cell entry (Letko et al., 2020; Yan et al., 2020a). S—a class I fusion protein—is also a critical determinant of viral host range and tissue tropism and the primary target of the host immune response (Li, 2016). As such, most coronavirus vaccine candidates are based on S or one of its sub-components. Coronavirus S glycoproteins contain three segments: a large ectodomain, a single-pass transmembrane anchor and a short intracellular tail. The ectodomain consists of a receptor-binding subunit, S1, which contains two sub-domains: one at the N-terminus and the other at the C-terminus. The latter comprises the receptor-binding domain (RBD), which serves the vital function of attaching the virus to the host receptor and triggering a conformational change in the protein that results in fusion with the host cell membrane through the S2 subunit.

Recently, the molecular structure of recombinant full-length SARS-CoV-2 Spike protein was solved in a stabilized pre-fusion state, by single particle cryo-Electron Microscopy (cryo-EM), at a resolution of 3.8 Å(Wrapp et al., 2020). Despite the comprehensive structural characterization of the spike protein as a whole, movement of the RBD between "up" and "down" conformational states prevented complete modeling of the RBD domains. Subsequent cryo-EM investigations of SARS-CoV-2 provided more detail of RBD, particularly at sites that contact the human ACE-2 receptor (Yan et al., 2020a). Here, we report the first high resolution—less than 2 Å—SARS-CoV-2 RBD. Additionally, we present the antigenicity of this recombinant RBD, particularly of interest, given the equipoise in the literature regarding the binding affinities of SARS-CoV antibodies for SARS-CoV-2 RBD. Early reports, have described that the human SARS-CoV antibody, CR3022, is able to bind to the SARS-CoV-2 RBD. In the present study, we verify binding, and subsequently solved the structure of SARS-CoV-2 RBD in complex with CR3022 with a novel "cryptic" epitope.

RESULTS

High resolution structure of the SARS-CoV-2 RBD

The SARS-CoV-2 RBD (residues 313-532), with a C-terminal His-tag, was expressed in 293F cells, and purified by NiNTA affinity, and size-exclusion chromatography. Crystallization condition screening identified 20% Jeffamine D2000, 10% Jeffamine M2005, 0.2 M NaCl, 0.1M MES pH 5.5 for diffraction quality crystal growth. Crystals diffracted to <1.8 Å in group P $4_1 2_1 2$ and to a complete dataset to 1.95 Å that could be scaled and processed (**Table 1**). The structure was refined to an R_{free} of 20% and R_{work} of 22% with no Ramachandran outliers. S residues 313-532 were clearly interpretable from the electron density map, with a dual conformation of a loop containing residues 484 to 487 clearly visible in the electron density map (**Figure 1**). Structure comparison of the unliganded RBD structure presented here, with the stabilized prefusion SARS-CoV-2 Spike (S-2P) molecule structure determined by Cryo-EM (PDB ID: 6VSB) (Wrapp et al., 2020) shows high structural similarity, with an RMSD of 0.68, 0.68, and 0.71 for each of the spike protomers. In the structure of the S-2P molecule (S-2P) (Wrapp et al., 2020) 25, 29 or 49

amino acids (aa) within each protomer RBD are not modeled, including 40% of the ACE-2 receptor binding site as measured by buried surface area (BSA)(Yan et al., 2020b). The SARS-CoV RBD-2 compared to liganded (PDB ID: 2AJF) and unliganded (PDB ID: 2GHV) SARS-CoV RBD structures shows high structural similarity, except for residues 473-488 (**Figure 1**). A chimeric SARS-CoV-2 RBD structure (PDB ID: 6VW1) with 23 aa differences compared to SARS-CoV-2, in complex with human ACE-2 was recently released in the PDB. Comparisons with previously published structures with the SARS-CoV-2 RBD highlight residues 473-488 as an area with significant structural plasticity. In the RBD structure from this study, we observe electron density for two conformations of the 482-486 loop. One of these conformations is highly similar to the ligand bound form of the RBD, while the second conformation would clash with the ACE2 receptor. Both this structural detail of the unliganded RBD and comparison to previously described RBD structures indicates that this area of the RBD is structurally malleable with implications for antibody or small molecule therapeutics design.

Identification of a set of cross-reactive SARS-CoV-2 antibodies

In an effort to identify antibodies that could bind to SARS-CoV-2, we screened a set of SARS-CoV,(Tripp et al., 2005) and MERS CoV(Wang et al., 2018; Wang et al., 2015) RBD-reactive antibodies for binding to the SARS-CoV-2 RBD. We demonstrated that the SARS-CoV mouse antibody 240CD (Tripp et al., 2005) had nanomolar (nM) affinity for the SARS-CoV-2 RBD and did not significantly block ACE-2 receptor binding (**Figure 2**). CR3022—a SARS-CoV neutralizing antibody (Tian et al., 2020) identified from a human phage-display library (ter Meulen et al., 2006)—also bound to SARS-CoV-2 RBD with nM affinity (**Figure 2B**). We assessed competition binding between 240CD and CR3022, and show that these antibodies cross-compete with each other for binding to the SARS-CoV-2 RBD (**Figure 2C, 2D**).

SARS-CoV-2 has a likely zoonotic origin and horseshoe bats have been implicated as natural reservoirs of both SARS-CoV and SARS-CoV-2 (Menachery et al., 2015; Zhou et al., 2020). As such, we next explored antibody cross-reactivity with the S glycoproteins of two bat SARS-related CoVs: SARSr-CoV Rs4874 (Ge et al., 2013; Yang et al., 2015) and Rs4231 (Hu et al., 2017), which are closely related to

the progenitor of SARS-CoV and retain the ability to utilize human ACE-2. CR3022 was able to recognize a recombinant Spike glycoproteins generated from bat SARSr-CoV Rs4874, while 240CD, and other mouse generated monoclonal antibodies have a mixed recognition phenotype (**Figure 2F**).

Crystal structure of antibody CR3022 in complex with SARS-CoV-2 RBD

The antigenic cross-reactivity of this set of antibodies precipitated an investigation into their molecular recognition determinants. The potential relevance of a human antibody motivated the investigation to prioritize studies of CR3022, for which a sequence was available (ter Meulen et al., 2006). The CR3022 heavy chain is encoded by IGHV5-51*03, contains a 12-aa CDR H3 with 8 V gene-encoded residues altered by somatic hypermutation. CR3022 light chain is encoded by IGKV4-1*01 with 1 V gene-encoded residue, altered by somatic hypermutation, and a 9-aa CDR L3 (**Extended Data Figure 2A**). To provide an atomic-level understanding of the structure of the CR3022 antibody, we crystallized the antigen-binding fragment (Fab) of CR3022. Crystals diffracted to 3.2 Å resolution in space group P 2_1 (**Table 1**). Overall the structure of the CR3022 Fab revealed a relatively flat antigen-combining site, with the exception of an extended protruding 12-aa CDR L1 loop (**Figure S2A**).

To determine the structure of CR3022 in complex with the SARS-CoV-2 RBD, we carried out crystallization conditions screening, with crystals of the CR3022-RBD complex forming in 1M Succinic acid, 0.1M Hepes pH 7, 2% PEG MME2000 and determined the crystal structure by X-ray diffraction to 4.25 Å (**Table 1**). The complex structure was solved by molecular replacement using the refined CR3022 and SARS-CoV-2 RBD structures as search models and was refined to an R_{work}/R_{free} of 0.242/0.292 (**Table 1**). CR3022 bound to the RBD at an epitope centered on S glycoprotein residues 377-386 with a total buried surface area of 871 Å (**Figure 3**, **Figure S2**, and **Table S1**). This region is highly conserved between SARS-CoV and SARS-CoV-2 (**Figure S3**). Comparison of the CR3022 epitope site with previously described antibody-complex structures for SARS-CoV, and MERS-CoV indicates that CR3022 describes a novel recognition site (**Figure 3** and **Figs. S3, S4**). Further sequence analysis of the epitope indicates that this epitope is conserved in betacoronavirus clade 2b, with also some similarity in clade 2d (**Fig. S3**). To confirm

that this site was also shared with 240CD, we produced an RBD knockout mutant by introducing a glycan sequon at position 384, and by biolayer interferometry show that both CR3022 and 240CD binding to the RBD can be eliminated by the introduction of a glycan at this site (**Fig. S2D**).

Identification of a cryptic site of vulnerability recognized by CR3022

The epitope conservation within the clade explains the antigenic cross-reactivity with both human SARS-CoV and bat SARS related CoV. To date, there has been extensive structural characterization of the SARS-CoV, and MERS-CoV spike molecule and domains, which provides a framework for understanding the novel SARS-CoV-2 spike molecule (**Table S2**). In the context of the coronavirus trimeric S glycoproteins, the RBD displays two prototypical conformations either in an "up" or "down" position, with implications for receptor binding and cell entry (**Table S1**). To further analyze these conformations, we modeled the CR3022 binding to the trimeric structures of SARS-CoV-2, SARS-CoV and MERS-CoV. The CR3022 epitope is occluded by adjacent spike protomers when the RBD is in the "down" conformation, but becomes more accessible when the spike is in a more open conformation here multiple RBD molecules are in the "up" conformation (**Figure 4**). There is still a clash of the antibody Fc1 region with the NTD from the same protomer, or an RBD from an adjacent protomer when modeled using the static structure.

To understand whether CR3022 could bind to SARS-CoV S glycoproteins, we measured binding to stabilized S-2P or non-stabilized versions of S (**Figure 4**). We observed robust binding to the non-stabilized S glycoprotein, while binding to SARS S-2P Trimer was low. We then treated the SARS S-2P trimer with trypsin and/or incubation with the ACE2 receptor to assess whether minimal proteolytic action or receptor binding could increase the availability of the "cryptic" CR3022 epitope. Incubation of the stabilized S-2P trimer with human ACE2 did not dramatically affect CR3022 binding, while in contrast, the trypsin treatment of the S-2P protein resulted in increased binding akin to the unstabilized S glycoprotein binding, and the level of binding was titratable, with increasing amounts of S-2P resulting in higher CR3022 binding. Given the prior neutralization and protection studies utilizing CR3022, and its

ability to complement potent neutralizing antibodies, it is likely that the CR3022 epitope represents a "cryptic" epitope that becomes exposed during the processes of viral cell entry.

In summary, our data represents the most detailed structural information for the SARS-CoV-2 RBD to date and the first structure of the SARS-CoV-2 in complex with a human antibody. The presence of "cryptic" but protective epitopes for influenza (Bangaru et al., 2019), and Ebola viruses (West et al., 2018), have been previously described. The identification of a novel "cryptic" epitope for betacoronaviruses including SARS-CoV, and SARS-CoV-2 highlight a novel viral vulnerability that can be harnessed in combination with ACE2 receptor site targeting monoclonal antibodies for vaccine and therapeutic countermeasure development.

Figure Legends

Figure 1. Crystal structure of the SARS-CoV-2 Receptor Binding Domain (RBD). A The SARS-CoV-2 RBD is shown in ribbon representation, glycan N343 is shown in stick representation, with the N- and C-termini shown as spheres. The Receptor-binding motif (residues 437-507) is colored forest green. **B** The SARS-CoV-2 RBD structure is overlaid with related structures including the incomplete RBD structure taken from the S-2P trimer structure (PDB ID: 6VSB), SARS-CoV RBD (PDB ID: 2AJF), and a chimeric SARS-CoV-2 RBD structure (PDB ID: 6VW1). **C** Close-up view of the membrane distal region of the RBD (residues 471-491). **D** Sequence alignment of SARS-CoV-2 and SARS-CoV RBDs. The RBD secondary structure is displayed above the sequence alignment Residues with significant structural difference > 2 Å are highlighted in purple.

Figure 2. Antigenic characterization of SARS-CoV-2 RBD. A,B, Binding kinetics of 240CD and CR3022 to SARS-CoV-2 RBD measured by biolayer interferometry. Kinetic constants were determined were calculated using a minimum of four dilutions of the RBD and fitted using a 1:1 binding model. **C,D,** Competition binding of antibodies CR3022 and 240CD to SARS-CoV-2 RBD. CR3022 or control antibody was allowed to bind to SARS-COV-2 prior to binding to 240CD or vice-versa. **E** SARS-CoV-2 RBD was sequentially bound by antibodies CR3022 or 240CD followed by soluble human ACE2 receptor. **F** SARS-CoV reactive antibodies were assessed for binding to bat SARS-related CoV Rs4784 and Rs4231 S glycoproteins.

Figure 3. Crystal structure of CR3022 in complex with SARS-CoV-2 RBD. A, RBD and CR3022 are shown in cartoon representation. **B** Structure of the SARS-CoV-2 RBD shown in surface representation. Residues which differ between SARS-CoV-2 and SARS-CoV are colored red. The CR3022 epitope is outlined in blue, and Thr-430 and Phe-384 located within the epitope are labeled. **C** The location of antibody CR3022, 230S, 80R, m396 and F26G19 epitopes and ACE-2 binding site on the RBD are outlined on the surface of the SARS-CoV-2 RBD.

Figure 4. Identification of CR3022 epitope as a "cryptic" epitope. Structural alignment of the SARS-CoV-2 RBD-CR3022 complex with the SARS-CoV S-2P structure. **A** The RBD-CR3022 structure is aligned to the SARS-CoV trimer structure (surface representation; PDB ID: 6CS1), where two RBD molecules are located in the "up" conformation. In this static structure, the Fc1 region of CR3022 (ribbon representation) clashes with the NTD of the same protomer. However, the epitope is fully accessible when more than one RBD is in the "up" representation. **B** Biolayer interferometry measurement of CR3022 binding to SARS S proteins with trypsin treatment or ACE2 receptor binding. **C** CR3022 binding to a serial dilution of SARS S-2P protein following trypsin treatment.

METHODS AND MATERIALS

Production of recombinant proteins

The Shanghai Public Health Clinical Center & School of Public Health, in collaboration with the Central Hospital of Wuhan, Huazhong University of Science and Technology, the Wuhan Center for Disease Control and Prevention, the National Institute for Communicable Disease Control and Prevention, Chinese Center for Disease Control, and the University of Sydney, Sydney, Australia released the sequence of a coronavirus genome from a case of a respiratory disease from Wuhan on January 10th available at recombinomics.co/topic/4351-wuhan-coronavirus-2019-ncov-sequences/. The sequence was also deposited in GenBank (accession MN908947) and GISAID (>EPI_ISL_402125). DNA encoding the SARS-Cov-2 RBD (residues 331-527) was synthesized (Genscript) with a C-terminal His6 purification tag and cloned into a CMVR plasmid, and protein was expressed by transient transfection in 293F cells for six days. The SARS-CoV-2 RBD-His protein was purified from cell culture supernatant using a Ni-NTA (Qiagen) affinity column. DNA encoding the S protein ectodomains (residues 1-1194) from bat SARS-related CoV isolates Rs4231 and Rs4874 (ref.(Hu et al., 2017)) were synthesized (Genscript) with a C-terminal T4-Foldon domain or C-terminal GCN domain, respectively, followed by factor xA cleavage sites and Strep-Tactin purification tags. Bat SARSr-CoV S genes were cloned into a modified pcDNA3.1 expression plasmid (Chan et al., 2009). Protein was initially expressed by transient transfection in 293F cells for six days, then serial cloned to select stably expressing cell lines (Yan L., in submission). The Rs4231-T4 and Rs4874-GCN S proteins were purified from cell culture supernatant using a Strep-Tactin affinity column. The oligomeric structure of these S proteins was selected by size exclusion chromatography (GE/AKTA) and trimeric S proteins were confirmed by Native-PAGE. SARS S-2P was produced as previously described, with Strep-Tactin affinity chromatography followed by gel filtration using a 16/60 Superdex-200 purification column. Purification purity for all S glycoproteins was assessed by SDS-PAGE.

The sequences of the CR3022 variable regions of the heavy and light chains are available in GenBank under accession numbers DQ168569 and DQ168570, respectively (ter Meulen et al., 2006). These

sequences were synthesized (Genscript) and cloned into CMVR expression vectors (NIH AIDS reagent program) between a murine Ig leader (GenBank DQ407610) and the constant regions of human IgG1 (GenBank AAA02914), Igκ (GenBank AKL91145). Plasmids encoding heavy and light chains were co-transfected into Expi293F cells (ThermoFisher) according to the manufacturer's instructions. After 5 days, antibodies were purified from cleared culture supernatants with Protein A agarose (ThermoFisher) using standard procedures, buffer exchanged into Phosphate-Buffered Saline (PBS), and quantified using calculated E and A280 measurements.

The Fab fragment of antibody CR3022 was prepared by digestion of the full-length IgG using enzyme Lys-C (Roche). The digestion reaction was allowed to proceed for 2.5 hours at 37°C. Digestion was assessed by SDS-PAGE and upon completion, the reaction mixture was passed through protein-G beads (0.5-1 ml beads), 3 times and the final flow through was assessed by SDS-PAGE for purity. The Fab fragment was mixed with purified SARS-CoV-2 RBD, and the complex was allowed to form for 1 hour at room temperature.

Sequence information:

SARS-CoV-2 RBD (signal peptide is underlined, purification tag in italics)

<u>MDSKGSSQKGSRLLLLLVVSNLLLPQGVVG</u>NITNLCPFGEVFNATRFASVYAWNRKRISNCVAD
YSVLYNSASFSTFKCYGVSPTKLNDLCFTNVYADSFVIRGDEVRQIAPGQTGKIADYNYKLPDDF
TGCVIAWNSNNLDSKVGGNYNYLYRLFRKSNLKPFERDISTEIYQAGSTPCNGVEGFNCYFPLQS
YGFQPTNGVGYQPYRVVVLSFELLHAPATVCG*PGSHHHHHH*

CR3022 Heavy chain Fv

EVQLVQSGTEVKKPGESLKISCKGSGYGFITYWIGWVRQMPGKGLEWMGIIYPGDSETRYSPSFQ
GQVTISADKSINTAYLQWSSLKASDTAIYYCAGGSGISTPMDVWGQGTTVTVSS

CR3022 Light chain Fv

DIVMTQSPDSLAVSLGERATINCKSSQSVLYSSINKNYLAWYQQKPGQPPKLLIYWASTRESGVP
DRFSGSGSGTDFTLTISSLQAEDVAVYYCQQYYSTPYTFGQGTKVEIK

Cell lines

Expi293F (ThermoFisher Scientific #A14527), and 293F cell lines were utilized in this study.

X-ray Crystallography

Crystallization

SARS-CoV-2 RBD at 10 mg/ml and 5 mg/ml in PBS buffer was screened for crystallization conditions using an Art Robbins Gryphon crystallization robot, 0.2 ul drops, and a set of 1200 crystallization conditions. Crystal drops were observed using a Jan Scientific UVEX-PS with automated UV and brightfield drop imaging robot. Crystals of the SARS-CoV-2 RBD grew after 24 hours in multiple conditions from the Molecular Dimensions MIDAS crystal screen, with diffraction-quality crystals seen in conditions B1, G1, F6, and H10. CR3022 Fab was screened for crystallization at 10.0 mg/ml and 5.0 mg/ml concentrations in PBS. Diffraction quality crystals grew after 48 hours in 0.1M Imidazole pH 6.5, 40% 2-propanol and 15% PEG 8,000. For the complex, CR3022 Fab and SARS-CoV-2 RBD were mixed in 1:1 molar ratio and crystallization drops were set-up at 8.0 and 4.0 mg/ml concentrations in PBS buffer as described above. Crystals grew in a crystallization condition containing 1M Succinic acid, 0.1M HEPES pH 7.0 and 2% PEG MME2000. Both, RBD alone and CR3022 Fab-RBD complex, crystals were harvested and cryo-cooled in their respective crystallization conditions plus 25% glycerol.

Diffraction data collection and processing

Single crystals were transferred to mother liquor containing 22% glycerol, and cryo-cooled in liquid nitrogen prior to data collection. Diffraction data for SARS-CoV-2 RBD were collected at Advanced Photon Source (APS), Argonne National Laboratory, NE-CAT ID24-C beamline, and measured using a Dectris Eiger 16M PIXEL detector. Crystals grown in MIDAS condition B1 (20% Jeffamine D2000, 10% Jeffamine M2005, 0.2 M NaCl, 0.1M MES pH 5.5) provided the highest resolution diffraction with spots visible to 1.8 Å. A complete dataset could be processed to 1.95 Å in space group P41212. CR3022 Fab crystals diffracted to 3.3 Å on NE-CAT ID24-C beamline. Diffraction data could be scaled in P21 space

group with 99.9% completeness. Diffraction data for CR3022 and SARS-CoV-2 RBD complex were collected on NE-CAT ID24-C beamline at Advanced Photon Source (APS), and measured using a Dectris Eiger 16M PIXEL detector. Diffraction data from multiple crystals were merged and scaled together to achieve a final resolution of 4.2 Å with overall completeness of 82.2%. Data collection statistics are reported in Table 1.

Structure solution and refinement

Phenix xtriage was used to analyze the scaled diffraction data produced from HKL2000 and XDS. Data was analyzed for completeness, Matthew's coefficient, twinning or pseudo-translational pathology. The structure of the SARS-CoV-2 RBD was determined by molecular replacement using Phaser and a search model of the SARS RBD (PDB ID: 2AJF, molecule C). CR3022 Fab crystal structure was determined by molecular replacement using Coxsackievirus A6 neutralizing antibody 1D5 (PDB ID: 5XS7) as a search model. The CR3022-RBD complex structure was determined by molecular replacement using the refined CR3022 and SARS-CoV-2 RBD structures as search models. Refinement was carried out using Phenix refine with positional, global isotropic B factor refinement, and defined TLS groups, with iterative cycles of manual model building using COOT. Structure quality was assessed with MolProbity. The final refinement statistics for all the structures are reported in Table 1. All structure figures were generated using PyMOL (The PyMOL Molecular Graphics System [DeLano Scientific]).

Structure comparisons

Weighing epitope sites based on antigen-antibody interactions

Epitope sites correspond to antigen sites that are in contact with the antibody in the antigen-antibody complex (i.e. all sites that have non-hydrogen atoms within 4 Å of the antibody). For a given epitope site, the weight, which characterizes the interaction between the epitope site and the antibody (improved based on (Bai et al., 2019)), was defined as:

$$w = \frac{1}{2}\left(\frac{n_c}{\langle n_c \rangle} + \frac{n_{nb}}{\langle n_{nb} \rangle}\right)$$

in which, n_c is the number of contacts with the antibody (i.e. the number of non-hydrogen antibody atoms within 4 Å of the site) ; n_{nb} is the number of neighboring antibody residues; $\langle n_c \rangle$ is the mean number of contacts n_c and $\langle n_{nb} \rangle$ is the mean number of neighboring antibody residues n_{nb} across all epitope sites. A weight of 1.0 is attributed to the average interaction across all epitope sites. Neighboring residue pairs were identified by Delaunay tetrahedralization of side-chain centers of residues (C_α is counted as a side chain atom, pairs further than 8.5 Å were excluded). Quickhull(Barber, 1996) was used for the tetrahedralization and Biopython PDB (Hamelryck and Manderick, 2003) to handle the protein structure.

In the SARS-CoV-2 and SARS-CoV-1 RBD comparison, residues were considered similar for the following residues pairs: RK, RQ, KQ, QE, QN, ED, DN, TS, SA, VI, IL, LM and FY.

Biolayer interferometry

Affinity kinetic interactions between SARS-CoV-2 RBD proteins and antibodies were monitored on an Octet RED96 instrument (FortéBio). After reference subtraction, binding kinetic constants were determined, from at least 4 concentrations of Fab, by fitting the curves to a 1:1 Langmuir binding model using the Data analysis software 9.0 (FortéBio). Antibodies were loaded at 30 ug/ml onto a AHC probe for 120 s followed by baseline incubation for 30-60 s.

To assess antibody competition, either 240CD or CR3022 or a non-specific control antibody CR1-07 was incubated with the SARS-CoV-2 RBD prior to assessment of binding to CR3022 or 240CD. Antibody concentration was 30 ug/ml. To assess binding of human ACE-2 receptor in the presence or absence of antibodies CR3022, or 240CD, RBD was loaded onto a HIS probe. The RBD was then sequentially incubated with either CR3022, 240CD or control antibody CR1-07 prior to incubation with human ACE-2 receptor.

CR3022 was loaded onto an AHC probe for 120s prior to incubation with SARS-CoV S glycoproteins (15 ug/ml) alone or pre-incubated with ACE2 protein. SARS S-2P protein was treated with 0.1% bovine pancreas trypsin for 10 minutes prior to binding to binding measurements. SARS Spike protein

was provided by BEI resources, Lot 768P152. Binding of CR3022 was also carried out against a series of concentrations of SARS S-2P which had been treated with 0.1% w/w bovine pancreatic trypsin.

DATA AVAILABILITY

The associated accession numbers for the coordinates and structure factors reported in this paper are being deposited to the PDB.

ADDITIONAL RESOURCES

None

DECLARATION OF INTERESTS

No potential conflict of interest was reported by the authors.

REFERENCES

Bai, H., Li, Y., Michael, N.L., Robb, M.L., and Rolland, M. (2019). The breadth of HIV-1 neutralizing antibodies depends on the conservation of key sites in their epitopes. PLoS Comput Biol *15*, e1007056.

Bangaru, S., Lang, S., Schotsaert, M., Vanderven, H.A., Zhu, X., Kose, N., Bombardi, R., Finn, J.A., Kent, S.J., Gilchuk, P.*, et al.* (2019). A Site of Vulnerability on the Influenza Virus Hemagglutinin Head Domain Trimer Interface. Cell *177*, 1136-1152 e1118.

Barber, C.B., D.P. Dobkin, and H. Huhdanpaa (1996). The quickhull algorithm for convex hulls. ACM Transactions on Mathematical Software *22*, 469-483.

Chan, Y.P., Yan, L., Feng, Y.R., and Broder, C.C. (2009). Preparation of recombinant viral glycoproteins for novel and therapeutic antibody discovery. Methods in molecular biology *525*, 31-58, xiii.

Ge, X.Y., Li, J.L., Yang, X.L., Chmura, A.A., Zhu, G., Epstein, J.H., Mazet, J.K., Hu, B., Zhang, W., Peng, C.*, et al.* (2013). Isolation and characterization of a bat SARS-like coronavirus that uses the ACE2 receptor. Nature *503*, 535-538.

Hamelryck, T., and Manderick, B. (2003). PDB file parser and structure class implemented in Python. Bioinformatics *19*, 2308-2310.

Hu, B., Zeng, L.P., Yang, X.L., Ge, X.Y., Zhang, W., Li, B., Xie, J.Z., Shen, X.R., Zhang, Y.Z., Wang, N.*, et al.* (2017). Discovery of a rich gene pool of bat SARS-related coronaviruses provides new insights into the origin of SARS coronavirus. PLoS pathogens *13*, e1006698.

Letko, M., Marzi, A., and Munster, V. (2020). Functional assessment of cell entry and receptor usage for SARS-CoV-2 and other lineage B betacoronaviruses. Nature microbiology.

Li, F. (2016). Structure, Function, and Evolution of Coronavirus Spike Proteins. Annual review of virology *3*, 237-261.

Lu, R., Zhao, X., Li, J., Niu, P., Yang, B., Wu, H., Wang, W., Song, H., Huang, B., Zhu, N.*, et al.* (2020). Genomic characterisation and epidemiology of 2019 novel coronavirus: implications for virus origins and receptor binding. Lancet *395*, 565-574.

Menachery, V.D., Yount, B.L., Jr., Debbink, K., Agnihothram, S., Gralinski, L.E., Plante, J.A., Graham, R.L., Scobey, T., Ge, X.Y., Donaldson, E.F.*, et al.* (2015). A SARS-like cluster of circulating bat coronaviruses shows potential for human emergence. Nature medicine *21*, 1508-1513.

Munster, V.J., Koopmans, M., van Doremalen, N., van Riel, D., and de Wit, E. (2020). A Novel Coronavirus Emerging in China - Key Questions for Impact Assessment. The New England journal of medicine *382*, 692-694.

ter Meulen, J., van den Brink, E.N., Poon, L.L., Marissen, W.E., Leung, C.S., Cox, F., Cheung, C.Y., Bakker, A.Q., Bogaards, J.A., van Deventer, E.*, et al.* (2006). Human monoclonal antibody combination against SARS coronavirus: synergy and coverage of escape mutants. PLoS Med *3*, e237.

Tian, X., Li, C., Huang, A., Xia, S., Lu, S., Shi, Z., Lu, L., Jiang, S., Yang, Z., Wu, Y.*, et al.* (2020). Potent binding of 2019 novel coronavirus spike protein by a SARS coronavirus-specific human monoclonal antibody. Emerging microbes & infections *9*, 382-385.

Tripp, R.A., Haynes, L.M., Moore, D., Anderson, B., Tamin, A., Harcourt, B.H., Jones, L.P., Yilla, M., Babcock, G.J., Greenough, T.*, et al.* (2005). Monoclonal antibodies to SARS-associated coronavirus (SARS-CoV): Identification of neutralizing and antibodies reactive to S, N, M and E viral proteins. Journal of Virological Methods.

Wang, L., Shi, W., Chappell, J.D., Joyce, M.G., Zhang, Y., Kanekiyo, M., Becker, M.M., van Doremalen, N., Fischer, R., Wang, N.*, et al.* (2018). Importance of Neutralizing Monoclonal Antibodies Targeting Multiple Antigenic Sites on the Middle East Respiratory Syndrome Coronavirus Spike Glycoprotein To Avoid Neutralization Escape. Journal of virology *92*.

Wang, L., Shi, W., Joyce, M.G., Modjarrad, K., Zhang, Y., Leung, K., Lees, C.R., Zhou, T., Yassine, H.M., Kanekiyo, M.*, et al.* (2015). Evaluation of candidate vaccine approaches for MERS-CoV. Nature communications *6*, 7712.

West, B.R., Moyer, C.L., King, L.B., Fusco, M.L., Milligan, J.C., Hui, S., and Saphire, E.O. (2018). Structural Basis of Pan-Ebolavirus Neutralization by a Human Antibody against a Conserved, yet Cryptic Epitope. mBio *9*.

Wrapp, D., Wang, N., Corbett, K.S., Goldsmith, J.A., Hsieh, C.L., Abiona, O., Graham, B.S., and McLellan, J.S. (2020). Cryo-EM structure of the 2019-nCoV spike in the prefusion conformation. Science.

Wu, F., Zhao, S., Yu, B., Chen, Y.M., Wang, W., Song, Z.G., Hu, Y., Tao, Z.W., Tian, J.H., Pei, Y.Y.*, et al.* (2020). A new coronavirus associated with human respiratory disease in China. Nature.

Yan, R., Zhang, Y., Guo, Y., Xia, L., and Zhou, Q. (2020a). Structural basis for the recognition of the 2019-nCoV by human ACE2. BiorXiv.

Yan, R., Zhang, Y., Li, Y., Xia, L., Guo, Y., and Zhou, Q. (2020b). Structural basis for the recognition of the SARS-CoV-2 by full-length human ACE2. Science.

Yang, X.L., Hu, B., Wang, B., Wang, M.N., Zhang, Q., Zhang, W., Wu, L.J., Ge, X.Y., Zhang, Y.Z., Daszak, P.*, et al.* (2015). Isolation and Characterization of a Novel Bat Coronavirus Closely Related to the Direct Progenitor of Severe Acute Respiratory Syndrome Coronavirus. Journal of virology *90*, 3253-3256.

Zhou, P., Yang, X.L., Wang, X.G., Hu, B., Zhang, L., Zhang, W., Si, H.R., Zhu, Y., Li, B., Huang, C.L.*, et al.* (2020). A pneumonia outbreak associated with a new coronavirus of probable bat origin. Nature.

Table 1 | Crystallographic Data Collection and Refinement Statistics

	SARS-CoV-2 RBD	CR3022 Fab	SARS-CoV-2 RBD + CR3022 Fab
PDB Code			
Data collection			
Space group	$P4_12_12$	$P2_1$	$P4_122$
Cell dimensions			
a, b, c (Å)	80.5.80.5,161.7	52.1, 201.0, 57.0	151.17, 151.17,192.9
α, β, γ (°)	90.0,90.0,90.0	90.0, 109.4.0, 90.0	90.0,90.0,90.0
Resolution (Å)	50.0-1.95 (2.02-1.95)	50.00-3.3 (3.42-3.30)	50.0-4.2 (4.35-4.20)
Reflection (uni/tot)	38,164/107,541	16,019/30,025	13,814/84,711
R_{sym} or R_{merge}	4.7 (79.3)	8.9 (28.0)	24.6 (108.8)
R_{pim}	3.1 (59.8)	6.3 (19.8)	9.4 (57.0)
$CC1/2$	98.9 (70.6)	99.1 (93.5)	98.2 (47.6)
$I / \sigma I$	18.9 (1.1)	10.2 (1.6)	5.57 (1.0)
Completeness (%)	96.8 (90.0)	96.5 (95.4)	82.2 (48.8)
Redundancy	2.8 (2.4)	1.9 (1.9)	6.1 (3.4)
Refinement			
Resolution (Å)	20.0-1.95	20.0-3.3	30.0-4.2
Reflections	29,582	15,999	11,120
R_{work} / R_{free}*	16.5/20.0	25.4/27.5	24.2/29.2
No. atoms			
Protein	1,596	6,579	4,928
Ligand/ion	97	-	28
Water	79	-	n/a
B-factors			
Protein	28.8	66.7	145.6
Ligand/ion	56.2	-	190.4
Water	45.3	-	n/a
Ramachandran			
Favored/Allowed/ Outliers	94.5/5.5/0.0	90.8/8.0/1.2	92.0/8.0/0.0
Bond lengths (Å)	0.007	0.015	0.003
Bond angles (°)	0.874	1.52	0.621

Values in parentheses are for highest-resolution shells.
* Rfree was calculated using ~5% randomly selected reflections.

Table S1. Buried surface area of CR3022 in complex with SARS-CoV-2 RBD

CR3022 residue	Bond type	Accessible Surface Area (Å²)	Buried Surface Area (Å²)
H:VAL 2		19.25	0.17
H:TYR 27		196.06	37.22
H:GLY 28		34.09	22.53
H:ILE 30		79.49	45.95
H:THR 31		76.77	68.33
H:TYR 32		41.83	27.89
H:TRP 33		35.57	30.13
H:TYR 52	H	47.89	42.20
H:SER 55		51.50	17.77
H:GLU 56		75.85	18.52
H:LYS 73		111.52	9.17
H:GLY 95		8.55	8.55
H:SER 96		44.82	41.38
H:GLY 97		22.94	19.42
H:ILE 98		141.28	32.06
H:SER 99		105.91	25.84
H:THR 100		59.53	27.12
H:PRO 100A		109.00	11.16
H:ASP 101	H	89.73	32.30
H:VAL 102		34.00	0.17
L:TYR 27D	H	89.10	48.45
L:SER 27F	H	93.53	34.65
L:ILE 28		113.30	84.10
L:ALA 30		8.96	0.67
L:TYR 32		59.28	31.23
L:TYR 49		70.36	36.26
L:TRP 50		111.12	54.43
L:THR 53		57.72	22.88
L:ARG 54		77.45	9.69
L:GLU 55	H	92.85	32.34
L:SER 56		102.51	0.44

SARS-CoV-2 RBD residue	Bond type	Accessible Surface Area (Å²)	Buried Surface Area (Å²)
A:TYR 369		89.63	43.79
A:ASN 370		109.19	26.31
A:PHE 374		39.48	7.06
A:SER 375		73.32	23.62
A:THR 376		34.77	7.37
A:PHE 377	H	70.41	64.16
A:LYS 378		81.20	66.58
A:CYS 379		47.55	44.69
A:TYR 380		56.89	44.21
A:GLY 381		77.51	75.98
A:VAL 382		27.99	25.04
A:SER 383		35.46	30.2
A:PRO 384		103.29	88.93
A:THR 385	H	109.91	63.9
A:LYS 386		112.50	65.4
A:LEU 390		47.38	22.93
A:PHE 392		19.18	5.95
A:ARG 408		159.50	5.51
A:PRO 412		34.93	1.0
A:ASP 428	H	114.22	33.26
A:PHE 429		16.72	2.10
A:THR 430		58.41	40.64
A:PHE 515		10.67	0.61
A:LEU 517	H	112.44	72.37
A:LEU 518		101.56	6.69

H: Hydrogen bond

Table S2 | Protein DataBank files of SARS-CoV, MERS-CoV, and SARS-CoV-2 S structures

Virus	PDB Title	PDB ID	PMID	Release year	Type
SARS-CoV	Crystal structure of the SARS-CoV Spike protein fusion core	1WNC	15345712	2004	x-ray
	Structure of a proteolitically resistant core from the severe acute respiratory syndrome coronavirus S2 fusion protein	2BEZ	15604146	2004	x-ray
	Structure of a Proteolytically Resistant Core from the Severe Acute Respiratory Syndrome Coronavirus S2 Fusion Protein	2BEQ	15604146	2004	x-ray
	Post-fusion hairpin conformation of the sars coronavirus spike glycoprotein	1WYY	15840526	2005	x-ray
	Structure of SARS coronavirus spike receptor-binding domain complexed with its receptor	2AJF	16166518	2005	x-ray
	Crystal Structure of SARS-CoV Spike Receptor-Binding Domain Complexed with Neutralizing Antibody	2DD8	16597622	2006	x-ray
	Crystal Structure of anti-SARS m396 Antibody	2G75	16597622	2006	x-ray
	Crystal structure of SARS spike protein receptor binding domain	2GHV	16954221	2006	x-ray
	Crystal structure of SARS spike protein receptor binding domain in complex with a neutralizing antibody, 80R	2GHW	16954221	2006	x-ray
	Crystal structure of SARS spike protein receptor binding domain	2GHV	16954221	2006	x-ray
	X-ray crystal structure of the SARS coronavirus spike receptor binding domain in complex with F26G19 Fab	3BGF	19324051	2008	x-ray
	Crystal structure of spike protein receptor-binding domain from the 2005-2006 SARS coronavirus civet strain complexed with human-civet chimeric receptor ACE2	3D0I	18448527	2008	x-ray
	Crystal structure of spike protein receptor-binding domain from the 2002-2003 SARS coronavirus human strain complexed with human-civet chimeric receptor ACE2	3D0G	18448527	2008	x-ray
	Crystal structure of spike protein receptor-binding domain from the 2002-2003 SARS coronavirus civet strain complexed with human-civet chimeric receptor ACE2	3D0H	18448527	2008	x-ray
	Crystal structure of spike protein receptor-binding domain from SARS coronavirus epidemic strain complexed with human-civet chimeric receptor ACE2	3SCL		2012	x-ray
	Crystal structure of spike protein receptor-binding domain from a predicted SARS coronavirus civet strain complexed with human-civet chimeric receptor ACE2	3SCK		2012	x-ray
	Crystal structure of spike protein receptor-binding domain from a predicted SARS coronavirus civet strain complexed with human receptor ACE2	3SCJ		2012	x-ray
	Crystal structure of spike protein receptor-binding domain from a predicted SARS coronavirus human strain complexed with human receptor ACE2	3SCI		2012	x-ray
	SARS-CoV spike glycoprotein	5WRG	28008928	2017	EM
	Structure of SARS-CoV spike glycoprotein	5XLR	28008928	2017	EM
	Structure of the N-terminal domain (NTD)of SARS-CoV spike protein	5X4S	28393837	2017	x-ray
	Prefusion structure of SARS-CoV spike glycoprotein, conformation 1	5X58	28393837	2017	EM
	Prefusion structure of SARS-CoV spike glycoprotein, conformation 2	5X5B	28393837	2017	EM
	Tectonic conformational changes of a coronavirus spike glycoprotein promote membrane fusion	6B3O	29073020	2017	EM
	Crystal Structure of the Human Coronavirus SARS HR1 motif in complex with pan-CoVs inhibitor EK1	5ZVM	30989115	2019	x-ray
	SARS Spike Glycoprotein, Stabilized variant, C3 symmetry	6CRV	30356097	2018	EM
	SARS Spike Glycoprotein, Stabilized variant, single upwards S1 CTD conformation	6CRW	30356097	2018	EM
	SARS Spike Glycoprotein, Stabilized variant, two S1 CTDs in the upwards conformation	6CRX	30356097	2018	EM
	SARS Spike Glycoprotein, Trypsin-cleaved, Stabilized variant, C3 symmetry	6CRZ	30356097	2018	EM
	SARS Spike Glycoprotein, Trypsin-cleaved, Stabilized variant, one S1 CTD in an upwards conformation	6CS0	30356097	2018	EM

SARS Spike Glycoprotein, Trypsin-cleaved, Stabilized variant, two S1 CTDs in an upwards conformation	6CS1	30356097	2018	EM
SARS Spike Glycoprotein - human ACE2 complex, Stabilized variant, all ACE2-bound particles	6CS2	30356097	2018	EM
Trypsin-cleaved and low pH-treated SARS-CoV spike glycoprotein and ACE2 complex, ACE2-free conformation with three RBD in down conformation	6ACC	30102747	2018	EM
Trypsin-cleaved and low pH-treated SARS-CoV spike glycoprotein and ACE2 complex, ACE2-free conformation with one RBD in up conformation	6ACD	30102747	2018	EM
Trypsin-cleaved and low pH-treated SARS-CoV spike glycoprotein and ACE2 complex, ACE2-bound conformation 1	6ACG	30102747	2018	EM
Trypsin-cleaved and low pH-treated SARS-CoV spike glycoprotein and ACE2 complex, ACE2-bound conformation 2	6ACJ	30102747	2018	EM
Trypsin-cleaved and low pH-treated SARS-CoV spike glycoprotein and ACE2 complex, ACE2-bound conformation 3	6ACK	30102747	2018	EM
Crystal Structure of the Human Coronavirus SARS HR1 motif in complex with pan-CoVs inhibitor EK1	5ZVM	30989115	2019	x-ray
SARS-CoV complex with human neutralizing S230 antibody Fab fragment (state 1)	6NB6	30712865	2019	EM
SARS-CoV complex with human neutralizing S230 antibody Fab fragment (state 2)	6NB7	30712865	2019	EM
Crystal structure of anti- SARS-CoV human neutralizing S230 antibody Fab fragment	6NB8	30712865	2019	EM
MERS-CoV				
Structure of the MERS-CoV fusion core	4MOD	24067982	2013	x-ray
Crystal structure of MERS-CoV complexed with human DPP4	4L72	23835475	2013	x-ray
Complex structure of MERS-CoV spike RBD bound to CD26	4KR0	23831647	2013	x-ray
structure of the receptor binding domain (RBD) of MERS-CoV spike	4KQZ	23831647	2013	x-ray
Bat-derived coronavirus HKU4 uses MERS-CoV receptor human CD26 for cell entry	4QZV	25211075	2014	x-ray
Crystal structure of middle east respiratory syndrome coronavirus S2 protein fusion core	4NJL	24473083	2014	x-ray
Receptor binding domain and Fab complex	4ZS6	26281793	2015	x-ray
Complex structure of MERS-RBD bound with 4C2 antibody	5DO2	26391698	2015	x-ray
Crystal structure of potent neutralizing antibody m336 in complex with MERS Co-V RBD	4XAK	26370782	2015	x-ray
Structure of MERS-Coronavirus Spike Receptor-binding Domain (England1 Strain) in Complex with Vaccine-Elicited Murine Neutralizing Antibody D12 (Crystal Form 1)	4ZPT	26218507	2015	x-ray
Structure of MERS-Coronavirus Spike Receptor-binding Domain (England1 Strain) in Complex with Vaccine-Elicited Murine Neutralizing Antibody D12 (Crystal Form 2)	4ZPV	26218507	2015	x-ray
Structure of unbound MERS-CoV spike receptor-binding domain (England1 strain).	4ZPW	26218507	2015	x-ray
Structure of the N-terminal domain (NTD) of MERS-CoV spike protein	5X4R	28393837	2017	x-ray
Prefusion structure of MERS-CoV spike glycoprotein, three-fold symmetry	5X59	28393837	2017	EM
Prefusion structure of MERS-CoV spike glycoprotein, conformation 1	5X5C	28393837	2017	EM
Prefusion structure of MERS-CoV spike glycoprotein, conformation 2	5X5F	28393837	2017	EM
Structure of MERS-CoV RBD in complex with a fully human antibody MCA1	5GMQ	28472421	2017	x-ray
Crystal Structure of MERS-CoV S1 N-terminal Domain	5VYH	28807998	2017	x-ray
Crystal Structure of MERS-CoV neutralizing antibody G4 Fab	5VZR	28807998	2017	x-ray
MERS S ectodomain trimer in complex with variable domain of neutralizing antibody G4	5W9H	28807998	2017	EM
MERS S ectodomain trimer in complex with variable domain of neutralizing antibody G4	5W9I	28807998	2017	EM
MERS S ectodomain trimer in complex with variable domain of neutralizing antibody G4	5W9J	28807998	2017	EM

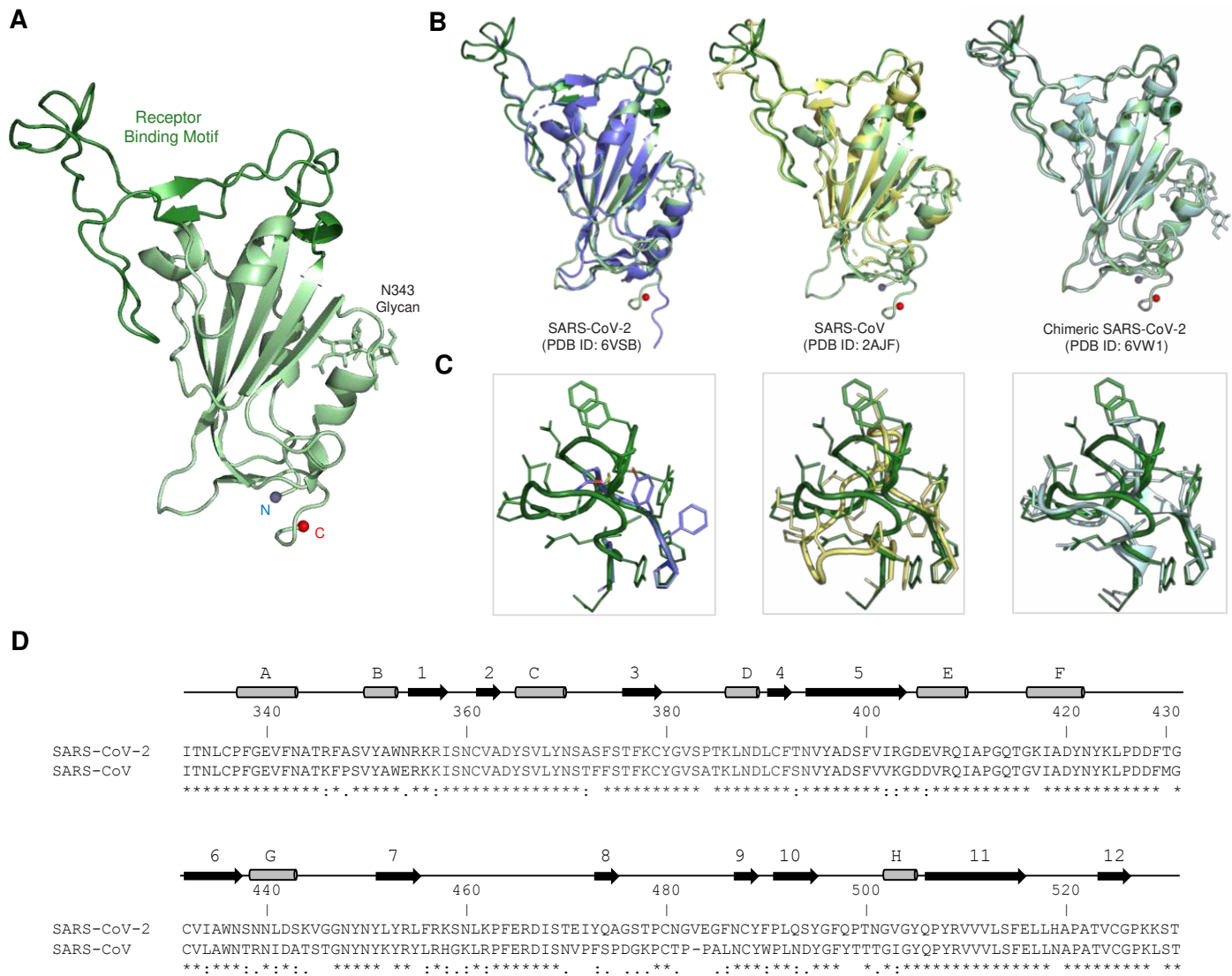|				
MERS S ectodomain trimer in complex with variable domain of neutralizing antibody G4	5W9K	28807998	2017	EM
MERS S ectodomain trimer in complex with variable domain of neutralizing antibody G4	5W9L	28807998	2017	EM
MERS S ectodomain trimer in complex with variable domain of neutralizing antibody G4	5W9M	28807998	2017	EM
MERS S ectodomain trimer in complex with variable domain of neutralizing antibody G4	5W9N	28807998	2017	EM
MERS S ectodomain trimer in complex with variable domain of neutralizing antibody G4	5W9O	28807998	2017	EM
MERS S ectodomain trimer in complex with variable domain of neutralizing antibody G4	5W9P	28807998	2017	EM
Crystal structure of Middle-East Respiratory Syndrome (MERS) coronavirus neutralizing antibody JC57-14 isolated from a vaccinated rhesus macaque in complex with MERS Receptor Binding Domain	6C6Y	29514901	2018	x-ray
Crystal structure of Middle-East Respiratory Syndrome (MERS) coronavirus neutralizing antibody JC57-14 isolated from a vaccinated rhesus macaque.	6C6X	29514901	2018	x-ray
Crystal structure of potent neutralizing antibody CDC2-C2 in complex with MERS-CoV S1 RBD	6C6Z	29514901	2018	x-ray
Structural definition of a unique neutralization epitope on the receptor-binding domain of MERS-CoV spike glycoprotein	5YY5	29996104	2018	x-ray
Structural definition of a unique neutralization epitope on the receptor-binding domain of MERS-CoV spike glycoprotein	5ZXV	29996104	2018	x-ray
MERS-CoV complex with human neutralizing LCA60 antibody Fab fragment (state 1)	6NB3	30712865	2019	EM
MERS-CoV S structure in complex with sialyl-lewisX	6Q05	31792450	2019	EM
MERS-CoV spike N-terminal domain and 7D10 scFv complex	6J11	31296843	2019	x-ray
MERS S0 trimer in complex with variable domain of antibody G2	6PZ8	31553909	2019	EM
Crystal Structure of MERS-CoV neutralizing antibody G2 Fab	6PXG	31553909	2019	x-ray
Crystal Structure of MERS-CoV S1-NTD bound with G2 Fab	6PXH	31553909	2019	x-ray
MERS-CoV S structure in complex with 5-N-acetyl neuraminic acid	6Q04	31792450	2019	EM
MERS-CoV S structure in complex with sialyl-lewisX	6Q05	31792450	2019	EM
MERS-CoV S structure in complex with 2,3-sialyl-N-acetyl-lactosamine	6Q06	31792450	2019	EM
MERS-CoV S structure in complex with 2,6-sialyl-N-acetyl-lactosamine	6Q07	31792450	2019	EM
Complex structure of bat CD26 and MERS-RBD	6L8Q		2019	x-ray
Crystal Structure of the Human Coronavirus MERS HR1 motif in complex with pan-CoVs inhibitor EK1	5ZVK	30989115	2019	x-ray
Crystal structure of anti- MERS-CoV human neutralizing LCA60 antibody Fab fragment	6NB5	30712865	2019	EM
MERS-CoV S complex with human neutralizing LCA60 antibody Fab fragment (state 2)	6NB4	30712865	2020	EM
SARS-CoV-2				
Prefusion 2019-nCoV spike glycoprotein with a single receptor-binding domain up	6VSB	32075877	2020	EM
Structure of the 2019-nCoV HR2 Domain	6LVN		2020	x-ray
Structure of post fusion core of 2019-nCoV S2 subunit	6LXT		2020	x-ray
Structural basis for receptor recognition by the novel coronavirus from Wuhan	6VW1		2020	x-ray
The 2019-nCoV RBD/ACE2-B0AT1 complex	6M17		2020	x-ray
Structure of the SARS-CoV-2 spike glycoprotein (closed state)	6VXX		2020	EM
SARS-CoV-2 spike ectodomain structure (open state)	6VYB		2020	EM

Figure 1

Figure 1. Crystal structure of the SARS-CoV-2 Receptor Binding Domain (RBD). A The SARS-CoV-2 RBD is shown in ribbon representation, glycan N343 is shown in stick representation, with the N- and C-termini shown as spheres. The Receptor-binding motif (residues 437-507) is colored forest green. **B** The SARS-CoV-2 RBD structure is overlaid with related structures including the incomplete RBD structure taken from the S-2P trimer structure (PDB ID: 6VSB), SARS-CoV RBD (PDB ID: 2AJF), and a chimeric SARS-CoV-2 RBD structure (PDB ID: 6VW1). **C** Close-up view of the membrane distal region of the RBD (residues 471-491). **D** Sequence alignment of SARS-CoV-2 and SARS-CoV RBDs. The RBD secondary structure is displayed above the sequence alignment Residues with significant structural difference > 2 Å are highlighted in purple.
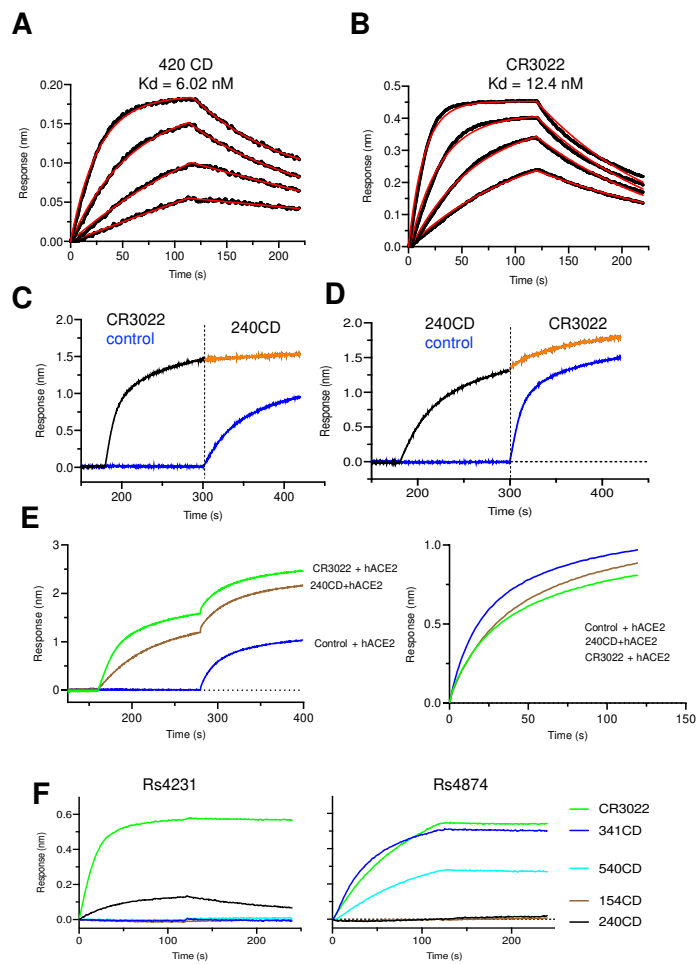
Figure 2

Figure 2. Antigenic characterization of SARS-CoV-2 RBD. A,B, Binding kinetics of 240CD and CR3022 to SARS-CoV-2 RBD measured by biolayer interferometry. Kinetic constants were determined were calculated using a minimum of four dilutions of the RBD and fitted using a 1:1 binding model. **C,D,** Competition binding of antibodies CR3022 and 240CD to SARS-CoV-2 RBD. CR3022 or control antibody was allowed to bind to SARS-COV-2 prior to binding to 240CD or vice-versa. **E** SARS-CoV-2 RBD was sequentially bound by antibodies CR3022 or 240CD followed by soluble human ACE2 receptor. **F** SARS-CoV reactive antibodies were assessed for binding to bat SARS-related CoV Rs4784 and Rs4231 S glycoproteins.
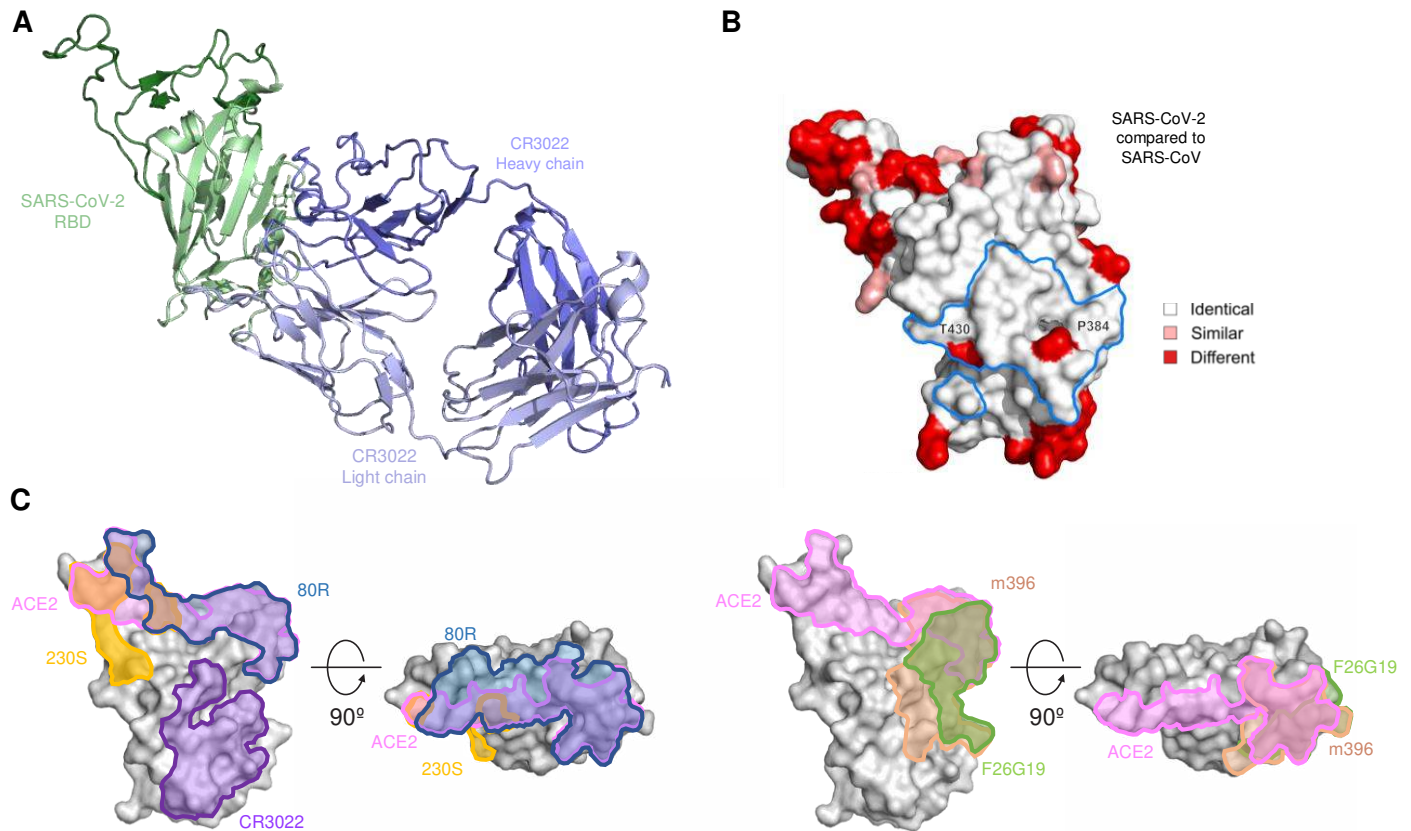
Figure 3

Figure 3. Crystal structure of CR3022 in complex with SARS-CoV-2 RBD. A, RBD and CR3022 are shown in cartoon representation. **B** Structure of the SARS-CoV-2 RBD shown in surface representation. Residues which differ between SARS-CoV-2 and SARS-CoV are colored red. The CR3022 epitope is outlined in blue, and Thr-430 and Phe-384 located within the epitope are labeled. **C** The location of antibody CR3022, 230S, 80R, m396 and F26G19 epitopes and ACE-2 binding site on the RBD are outlined on the surface of the SARS-CoV-2 RBD.
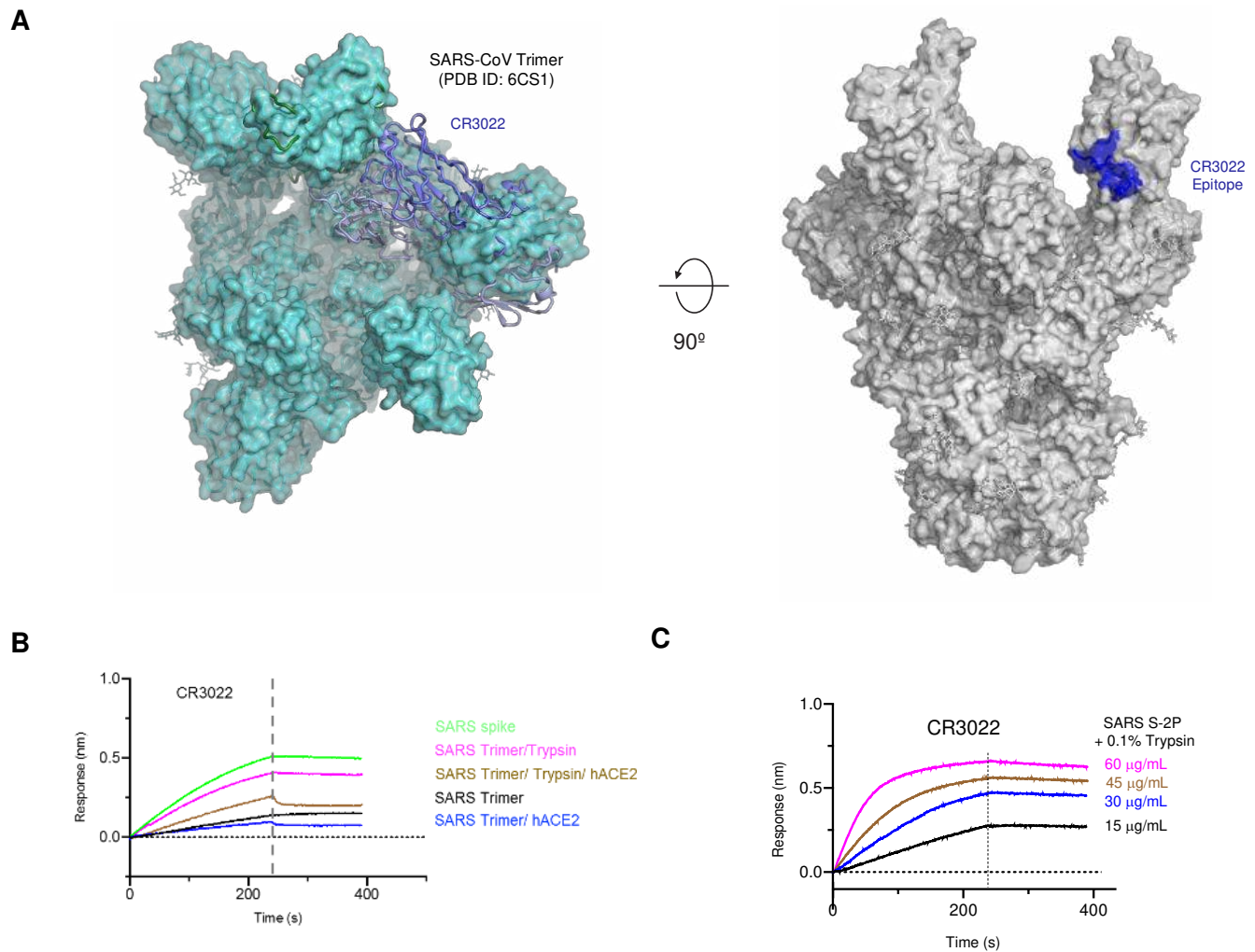
Figure 4

Figure 4. Identification of CR3022 epitope as a "cryptic" epitope. Structural alignment of the SARS-CoV-2 RBD-CR3022 complex with the SARS-CoV S-2P structure. **A** The RBD-CR3022 structure is aligned to the SARS-CoV trimer structure (surface representation; PDB ID: 6CS1), where two RBD molecules are located in the "up" conformation. In this static structure, the Fc1 region of CR3022 (ribbon representation) clashes with the NTD of the same protomer. However, the epitope is fully accessible when more than one RBD is in the "up" representation. **B** Biolayer interferometry measurement of CR3022 binding to SARS S proteins with trypsin treatment or ACE2 receptor binding. **C** CR3022 binding to a serial dilution of SARS S-2P protein following trypsin treatment.

```
SARS-CoV-2-spike    SETKCTLKSFTVEKGIYQTSNFRVQPTESIVRFPNITNLCPFGEVFNATRFASVYAWNRK        356
batRs4231-spike     AELKCSVKSFEIDKGIYQTSNFRVAPSKEVVRFPNITNLCPFGEVFNATTFPSVYAWERK        343
batWIV16-spike      AELKCSVKSFEIDKGIYQTSNFRVAPSKEVVRFPNITNLCPFGEVFNATTFPSVYAWERK        343
SARS-CoV-spike      AELKCSVKSFEIDKGIYQTSNFRVVPSGDVVRFPNITNLCPFGEVFNATKFPSVYAWERK        343
                                    ********** * *****:**

SARS-CoV-2-spike    RISNCVADYSVLYNSASFSTFKCYGVSPTKLNDLCFTNVYADSFVIRGDEVRQIAPGQTG        416
batRs4231-spike     RISNCVADYSVLYNSTSFSTFKCYGVSATKLNDLCFSNVYADSFVVKGDDVRQIAPGQTG        403
batWIV16-spike      RISNCVADYSVLYNSTSFSTFKCYGVSATKLNDLCFSNVYADSFVVKGDDVRQIAPGQTG        403
SARS-spike          KISNCVADYSVLYNSTFFSTFKCYGVSATKLNDLCFSNVYADSFVVKGDDVRQIAPGQTG        403
                    :*************: ********* ********:*********::**:**********

SARS-CoV-2-spike    KIADYNYKLPDDFTGCVIAWNSNNLDSKVGGNYNYLYRLFRKSNLKPFERDISTEIYQAG        476
batRs4231-spike     VIADYNYKLPDDFLGCVLAWNTNSKDSSTSGNYNYLYRWVRRSKLNPYERDLSNDIYSPG        463
batWIV16-spike      VIADYNYKLPDDFTGCVLAWNTRNIDATQTGNYNYKYRSLRHGKLRPFERDISNVPFSPD        463
SARS-spike          VIADYNYKLPDDFMGCVLAWNTRNIDATSTGNYNYKYRYLRHGKLRPFERDISNVPFSPD        463
                     ************ ***:***:.. *:.  ***** ** .*:.:*.*:***:*.  :. .

SARS-CoV-2-spike    STPCNGVEGFNCYFPLQSYGFQPTNGVGYQPYRVVVLSFELLHAPATVCGPKKSTNLVKN        536
batRs4231-spike     GQSCSA-IGPNCYNPLRPYGFFTTAGVGHQPYRVVVLSFELLNAPATVCGPKLSTDLIKN        522
batWIV16-spike      GKPCTP-PAFNCYWPLNDYGFYITNGIGYQPYRVVVLSFELLNAPATVCGPKLSTDLIKN        522
SARS-spike          GKPCTP-PALNCYWPLNDYGFYTTTGIGYQPYRVVVLSFELLNAPATVCGPKLSTDLIKN        522
```

Fig. S1. Sequence alignment of the receptor binding domain of SARS-CoV and related betacoronaviruses measured by Biolayer Interferometry for reactivity to SARS-CoV antibodies.
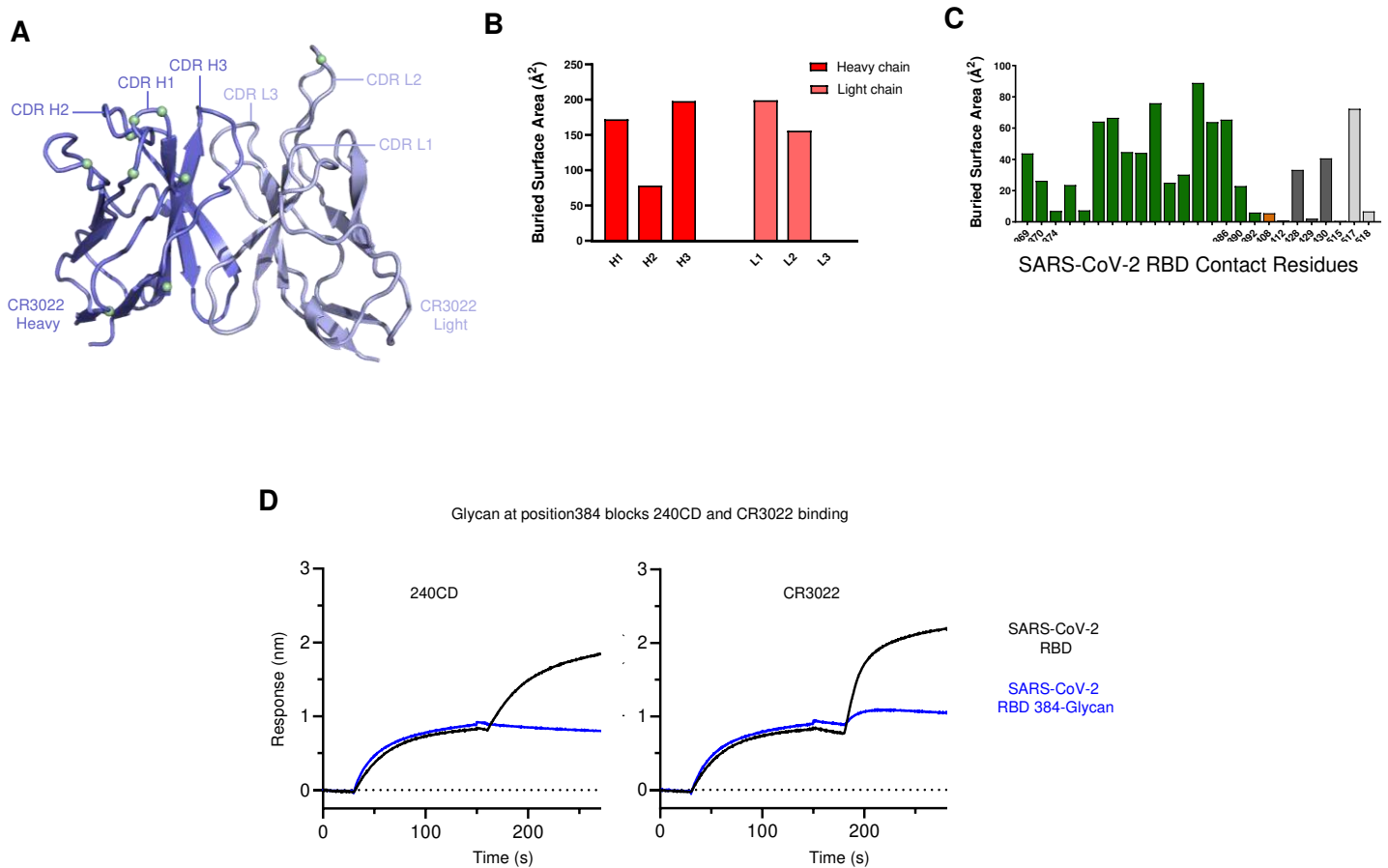
Fig. S2. CR3022 Fab crystal structure and epitope analysis. A CR3022 is shown in ribbon representation, with CDR loops indicated. Residues which have undergone somatic hypermutation are indicated with green spheres. **B** Heavy and light chain CDR loops paratope buried surface area. **C** Buried surface area analysis of the CR3022 epitope on the SARS-CoV-2 RBD. **D** Antibody binding to SARS-CoV-2 RBD and RBD with a glycan at position 384. RBD is initially loaded onto the HIS probe, followed by incubation with RBD variants.
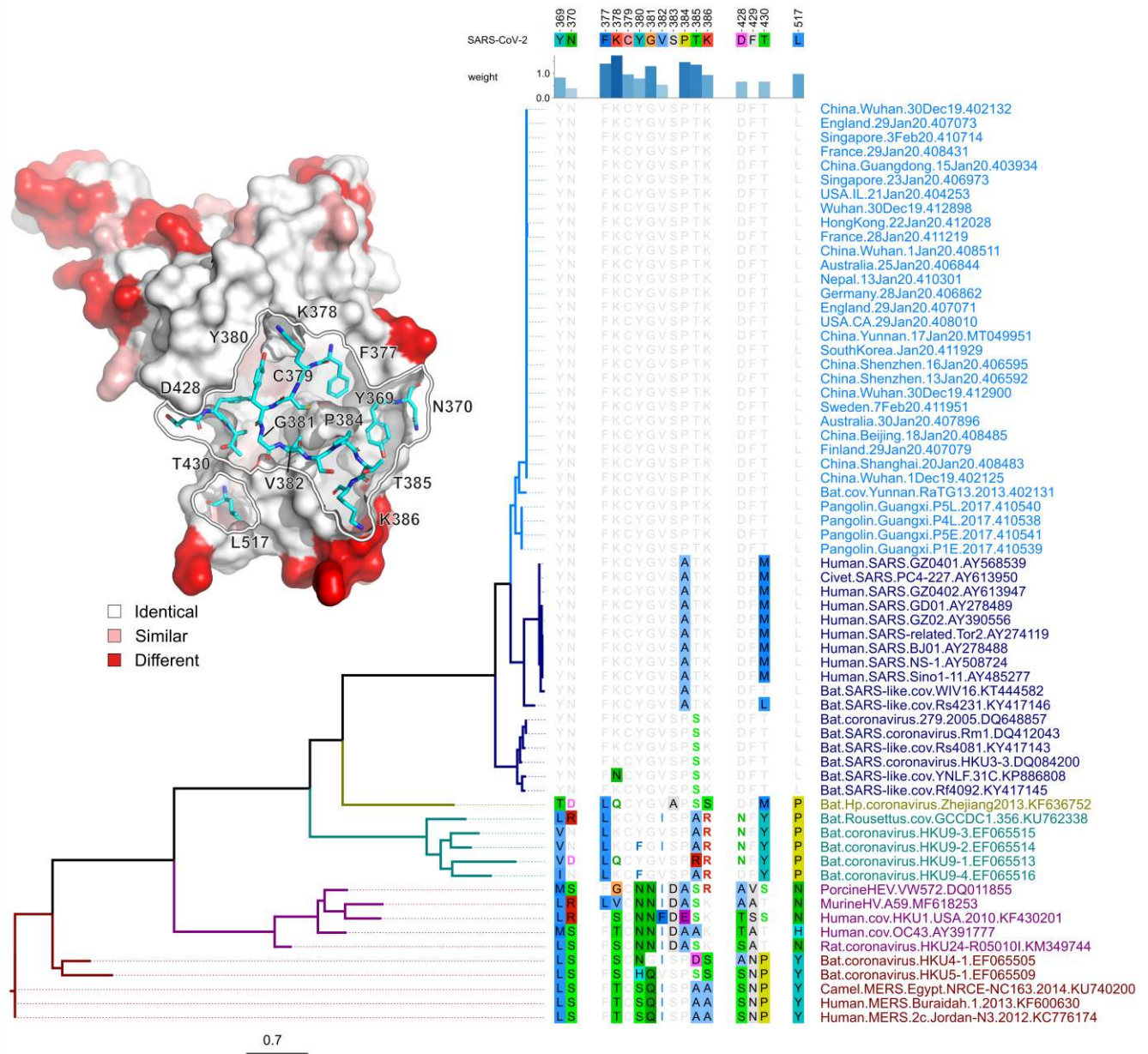
Fig. S3. Structural and sequence analysis of the CR3022 epitope. Analysis of the CR3022 footprint across betacoronaviruses. The CR3022 epitope on SARS-CoV-2 (China.Wuhan.30Dec19.402132) RBD is compared across betacoronaviruses. The epitope is numbered according to the Wuhan reference; the strength of the interaction between the Ab and the spike protein is indicated by the height and color of the histogram bars above the sequence alignment. Sequences are ordered based on their phylogenetic relationships based on a maximum likelihood phylogenetic tree derived from amino acid RBD sequences. The RBD structure is shown in surface representation and depicts mutations between SARS-CoV-1 and SARS-CoV-2 in red; the CR3022 epitope is outlined in white, with contact residues shown in stick representation.
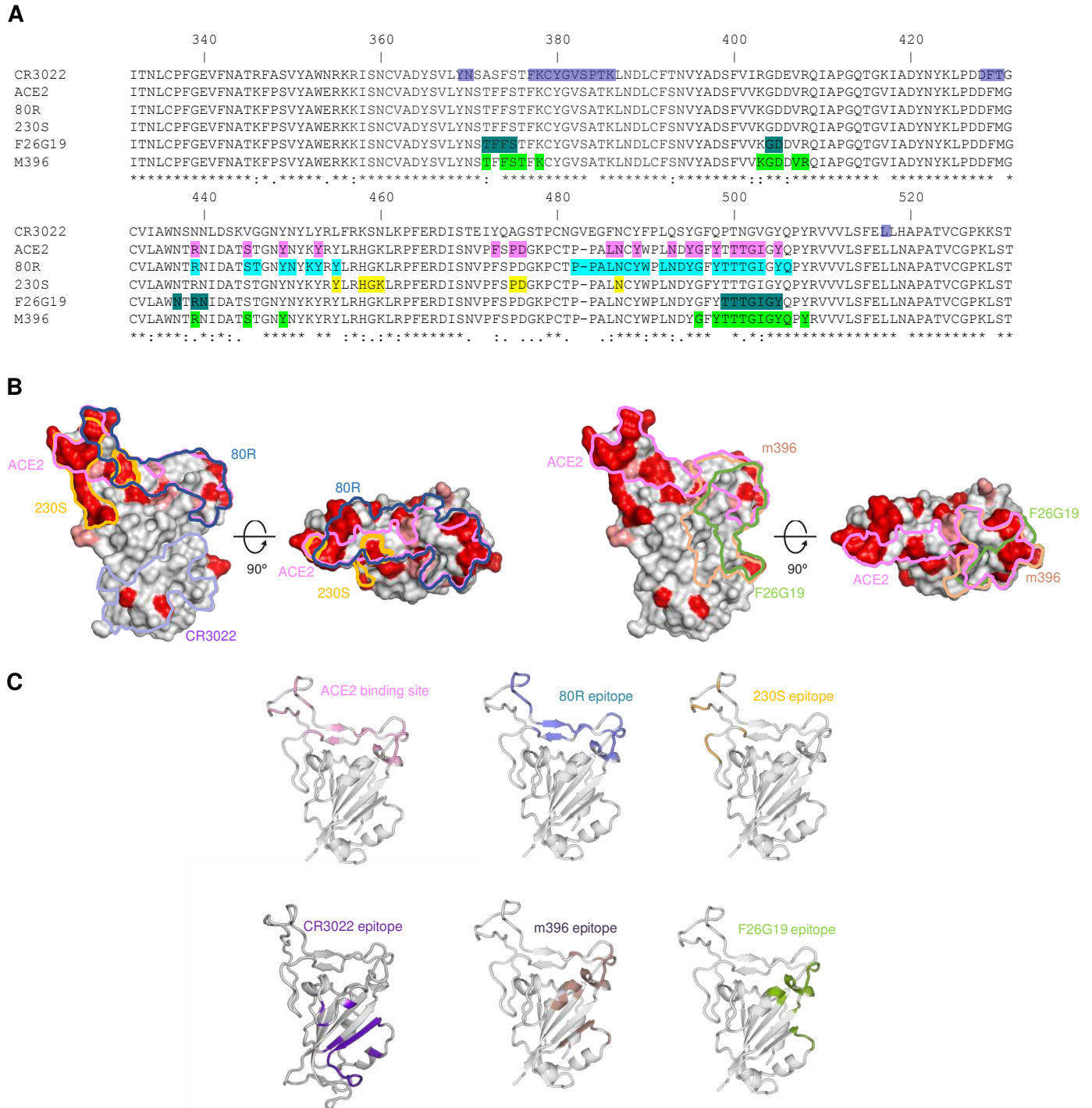
A

B

C

Fig. S4. SARS-CoV-2 and SARS-CoV antibody epitope analysis. A Sequence alignment of SARS-CoV-2 and SARS-CoV RBD. Antibody and ACE2 receptor interacting residues are highlighted on the sequence. **B** Antibody epitopes and receptor binding sites are outlined on the surface of the SARS-CoV RBD structures. The Sequence differences between SARS-COV-2 and SARS-CoV are indicated by red coloring on the RBD surface. **C** Antibody epitopes are shown on the SARS-CoV RBD molecule depicted in ribbon representation. The CR3022 epitope is shown on the SARS-CoV-2 RBD molecule.